Journal of Inorganic Biochemistry 112 (2012) 39–48

Contents lists available at SciVerse ScienceDirect

Journal of Inorganic Biochemistry

journal homepage: www.elsevier.com/locate/jinorgbio

Synthesis and characterization of unsymmetrical oxidovanadium complexes: DNA-binding, cleavage studies and antitumor activities

Jiazheng Lu [a,*], Haiwei Guo [a], Xiandong Zeng [a], Yongli Zhang [b,*], Ping Zhao [d], Jing Jiang [a,c], Linquan Zang [a]

[a] School of Pharmacy, Guangdong Pharmaceutical University, Guangzhou, 510006, People's Republic of China
[b] school of basic courses, Guangdong Pharmaceutical University, Guangzhou, 510006, People's Republic of China
[c] State Key Laboratory of Optoelectronic Material and Technologies & School of Chemistry and Chemical Engineering, Sun Yat-Sen University, Guangzhou, 510275, People's Republic of China
[d] School of Medicine Chemistry and Chemical Engineering, Guangdong Pharmaceutical University, Guangzhou, 510006, People's Republic of China

ARTICLE INFO

Article history:
Received 7 October 2011
Received in revised form 17 February 2012
Accepted 20 February 2012
Available online 13 March 2012

Keywords:
Oxidovandium complexes
DNA-binding
Cleavage
Antitumor

ABSTRACT

Four oxidovanadium(IV) complexes, [VO(hntdtsc)(phen)] (**1**), [VO(hntdtsc)(bpy)] (**2**) (hntdtsc = 2-hydroxy-1-naphthaldehyde thiosemicarbazone, phen = 1,10-phenanthroline), [VO(satsc)(phen)] (**3**) and [VO(satsc)(bpy)] (**4**) (satsc = salicylaldehyde thiosemicarbazone, bpy = 2,2′-bipyridine) have been synthesized and characterized. The results show that complexes **1**, **2**, **3** and **4** interact with DNA through intercalative mode and can efficiently cleave the plasmid pBR 322 DNA. It is interesting to note that these four complexes present highly cytotoxic activities against Myeloma cell (Ag8.653) and Gliomas cell (U251) lines. Complex **1** was found to be the most potent antitumor agent among the four complexes.

1. Introduction

In past decade, a number of transition metal complexes have been exploited for the design of new drugs due to their diverse biological activities. In particular for those containing polyaromatic ligands, great interest has been aroused on them owing to their usage as DNA-structural probes, DNA-dependent electron transfer and sequence-specific cleaving agents and potential anti-cancer drugs [1–4]. In fact, most of these properties have been found to be a direct bearing on the complexes binding DNA and cleaving DNA [5–8]. DNA-binding metal complexes, especially those with small molecular weight, have been extensively studied as DNA structural and conformational probes, DNA-dependent electron transfer and sequence-specific cleaving agents, and potential anti-cancer drugs [9–13].

As one of the trace bioelements existing in the human body, vanadium complexes have been found to present antibacterial, antitumor, insulin-enhancing and antiparasitic effects [14–16]. This bioelement takes part in various DNA maintenance reactions and thereby prevents genomic instability which otherwise leads to cancer [15,17]. Vanadium complexes could also suppress the growth and spread of existing tumors by inhibiting tumor cell proliferation, inducing apoptosis and limiting the invasion and metastatic potential of neoplastic cells [18,19]. Thus, the DNA-binding and antitumor activities of oxidovandium complexes based on vanadium-metal and multifunctional bridging ligands have been investigated [17,20,21]. On the other hand, Schiff bases have also been extensively studied because of their potential antibacterial, antifungal, anti-malarial and anticancer activities [16,18,22]. Moreover, the electronic effects of Schiff base complexes are also important and significant to carry out some discussions in this field in order to design complexes with better DNA-binding characteristics [23–25]. The presence of a rigid aromatic system in the Schiff base structure gives rise to particular spectroscopic properties, which make it a potential probe for nucleic acids. Because of their wide range of pharmacological applications, thiosemicarbazones were often chosen as such ligands for vanadium [16–19]. Additionally, thiosemicarbazones can bind to the nitrogen bases of DNA and so hinder or block base replication and create lesions in DNA strands by oxidative rupture [18,25–27]. So far, vanadyl complexes incorporating thiosemicarbazones have been studied extensively for their insulin-like effects which result in the inhibition of glycerol release and enhancement of glucose uptake by rat adipocytes and have been used in the treatment of tuberculosis [16,27,28]. In this context, it occurred to us that utilization of intercalate moiety of thiosemicarbazones in coordinate with vanadium might accentuates the biochemical activity of the so-derived hybrids molecules, which may lead to an efficient DNA binding and DNA cleavage. These oxidovanadium complexes may be a promising and attractive approach in the search for new potential drugs for the therapy of cancer [16,17].

* Corresponding authors. Tel.: +86 20 39352122; fax: +86 20 39352129.
E-mail address: lujia6812@163.com (J. Lu).

0162-0134/$ – see front matter © 2012 Elsevier Inc. All rights reserved.
doi:10.1016/j.jinorgbio.2012.02.034

In the present work, four oxidovanadium complexes, [VO(hntdtsc)(phen)] (**1**), [VO(hntdtsc)(bpy)] (**2**) (hntdtsc = 2-hydroxy-1-naphthaldehyde thiosemicarbazone, phen = 1,10-phenanthroline), [VO(satsc)(phen)] (**3**) and [VO(satsc)(bpy)] (**4**) (satsc = salicylaldehyde thiosemicarbazone, bpy = 2,2′-bipyridine) (see Scheme 1), have been synthesized and characterized by elemental analysis, UV–vis, ES-MS, IR, ^{1}H NMR and magnetic moment measurement. The interactions of these four complexes with calf-thymus DNA (CT-DNA) were investigated using UV–vis absorption titration, fluorescence spectra, viscosity measurements and thermal denaturation. Their photocleavage reactions with pBR322 supercoiled plasmid DNA were investigated by gel electrophoresis. In addition, the cytotoxicity of these four complexes against the Myeloma cell (Ag8.653) and Gliomas cell (U251) was assessed by MTT assay.

2. Materials and methods

2.1. Materials

VO (acac) $_2$ (acac = acetylacetonate), 1,10-phenanthroline and 2,2′-dipyridyl were purchased from Shang hai jingchun company. CT-DNA and pBR 322 DNA were obtained from Sigma. Other materials were obtained from commercial sources and used as received (analytical reagents). Tris–HCl buffer A (5 mM Tris (hydroxymetylaminomethane)–HCl, 50 mM NaCl, pH = 7.2) was used for absorption titration, luminescence titration, and viscosity experiments. Tris–HCl buffer B (50 mM Tris–HCl and 18 mM NaCl, pH = 7.2) was used for DNA-cleavage experiments. Buffer C (1.5 mM $NaHPO_4$, 0.5 mM NaH_2PO_4 and 0.25 mM Na_2H_2EDTA (pH = 7.0)) was used for thermal denaturation. All buffers were prepared using double-distilled water. A solution of CT-DNA in the buffer gave a ratio of UV absorbance at 260 and 280 nm of ca. 1.8–1.9, indicating that the DNA was sufficiently free of protein [29–34]. The DNA concentration per nucleotide was determined by absorption spectroscopy using the molar absorptivity (6600 M^{-1} cm^{-1}) at 260 nm [28,29,34]. Flash chromatography was performed using silica gel (200–300 mesh). Unless otherwise stated, reagents were commercially available and of analytical grade.

2.2. Physical measurements

Microanalysis (C, H, and N) was carried out with a Perkin-Elmer 240Q elemental analyzer. Electrospray mass spectra (ES-MS) were recorded on a LCQ system (Finnigan MAT, USA) using methanol as mobile phase. The spray voltage, tube lens offset, capillary voltage and capillary temperature were set at 4.50 kV, 30.00 V, 23.00 V and 200 °C, respectively, and the quoted m/z values are for the major peaks in the isotope distribution. ^{1}H NMR spectra were recorded on a Varian-500 spectrometer. All chemical shifts are given relative to tetramethylsilane (TMS). Infrared spectra were recorded on a Bomen FTIR model MB102 instrument using KBr pellets. UV/Vis spectra were recorded on a Shimadzu UV-3101 PC spectrophotometer at room temperature. Emission spectra were recorded on a Perkin-Elmer Lambda 55 spectrofluorophotometer. Magnetic susceptibility measurements were recorded on a MPMSXL-7(Quantum Design, USA), at room temperature. Molar conductivities in DMF (1 mM/L) solution at room temperature were measured using DDS-307 digital direct reading conductivity meter.

2.3. Synthesis of the ligands and complexes

2.3.1. Synthesis of 2-hydroxy-1-naphthaldehyde thiosemicarbazone (**hntdtsc**)

hntdtsc was synthesized through a modification of a previously reported procedure [33–36]. A stirring solution of 2-hydroxy-1-naphthaldehyde (0.8609 g, 5 mmol) in 10 mL of absolute alcohol was added dropwise to thiosemicarbazide (0.4557 g, 5 mmol)

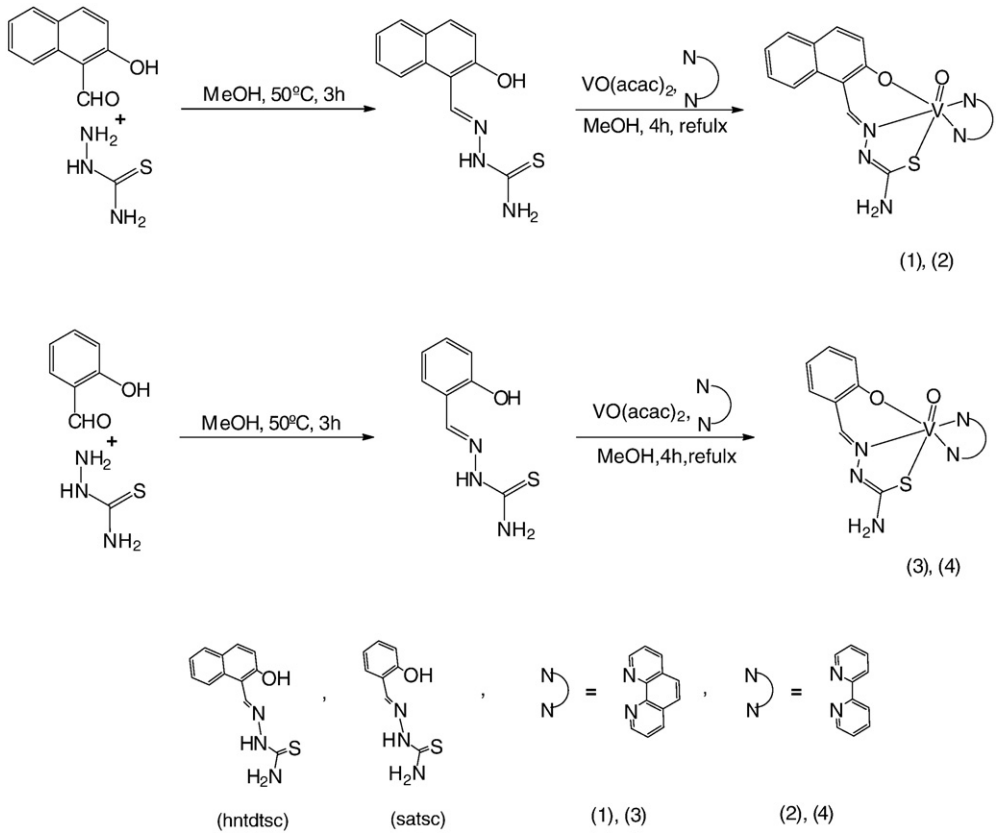

Scheme 1. Synthesis of ligands and complexes.

which was dissolved in 10 mL of absolute alcohol, then the mixture was continuously stirred at 50 °C for 3 h and gave a white gossypine precipitate, which was used without further purification. Yield: 88%. Anal. Calcd. for $C_{12}H_{11}N_3OS$: C, 58.76; H, 4.52; N, 17.13; S, 13.07%; Found: C, 58.70; H, 4.61; N, 17.08; S, 13.01%. ES-MS (CH_3OH, m/z): 246.0 (100%) ($[M+1]^+$). IR (KBr) (ν_{max}/cm^{-1}): 3450 (vs), 3253 (vs, $-NH_2$), 3167 (vs, N–H), 3053 (m, C–H), 1625 (s), 1593 (vs), 1572 (s), 1509 (vs), 1472 (s), 1452 (m), 1033 (m, C–N), 1240 (s, C–O), 821 (s), 753 (s, C═S). ^{1}H NMR (500 MHz, DMSO-d_6): 11.42 (s, 1H, NHCS), 10.51 (s, 1H, OH), 9.06 (s, 1H, CH═N), 7.85 and 8.25 (2br s, 1H,NH_2), 8.53 (d, 1H, ArH, $J=8.7$ Hz), 7.89 (d, 1H, ArH, $J=7.6$ Hz), 7.86 (d, 1H, ArH, $J=8.2$ Hz), 7.57 (t, 1H, ArH, $J=8.0$ Hz), 7.38 (t, 1H, ArH, $J=7.6$ Hz), 7.21 (d, 1H, ArH, $J=8.4$ Hz). UV–vis λ_{max}, nm (ε, $M^{-1}\,cm^{-1}$) in DMSO: 342 (25,320).

2.3.2. Synthesis of salicylaldehyde thiosemicarbazone (**satsc**)

This compound was prepared by a similar procedure as for the compound hntdtsc, with salicylaldehyde (0.6106 g, 5 mmol) in place of 2-hydroxy-1-naphthaldehyde and gave a white precipitate, which was used without further purification. Yield: 56%. Anal. Calcd. for $C_8H_9N_3OS$: C, 49.21; H, 4.65; N, 21.55; S, 16.42%; Found: C, 49.13; H, 4.69; N, 21.53; S, 16.39%. ES-MS (CH_3OH, m/z): 196.0 (100%) ($[M+1]^+$). IR (KBr) (ν_{max}/cm^{-1}): 3444 (vs), 3321 (vs, $-NH_2$), 3175 (vs, N–H), 3033 (m, C–H), 1627 (vs), 1537 (vs), 1491 (s), 1465 (s), 1237 (m, C–O), 1036 (m, C–N), 830 (s), 752 (s, C═S). ^{1}H NMR (500 MHz, DMSO-d_6): 11.40 (s, 1H, NHCS), 9.89 (s, 1H, OH), 8.38 (s, 1H, CH═N), 7.92 and 8.13 (2br s, 1H each NH_2), 7.92 (s, 1H, ArH), 7.21(t, 1H, ArH, $J=8.4$ Hz), 6.88 (d, 1H, ArH, $J=7.8$ Hz), 6.81 (t, 1H, ArH, $J=8.2$ Hz). UV–vis λ_{max}, nm (ε, $M^{-1}\,cm^{-1}$) in DMSO: 340 (26,310).

2.3.3. Synthesis of [VO (hntdtsc) (phen)] (**1**)

A mixture of hntdtsc (0.1225 g, 0.5 mmol) and 1, 10-phennanthroline (0.0901 g, 0.5 mmol) in absolute methanol (100 mL) was heated at 80 °C under argon for 2 h. After dissolution, a 10 mL of methanol solution of VO $(acac)_2$ (0.1325 g, 0.5 mmol) was added dropwise to this mixture. The mixture was refluxed for another 4 h to give a reddish-brown precipitate. The solid powder was isolated from the hot solution and washed with absolute methanol and diethyl ether respectively, and dried in vacuo. Yield: 85.2%. Anal. Calcd. for $C_{24}H_{17}N_5O_2SV$: C, 58.78; H, 3.49; N, 14.28; S, 6.54%; Found: C, 58.71; H, 3.67; N, 14.26; S, 6.52%. ES-MS (CH_3OH, m/z): 491.0 (96%) ($[M+1]^+$). IR (KBr) (ν_{max}/cm^{-1}): 3436 (s), 3265 (m, $-NH_2$), 3047 (m, C–H), 1606 (vs), 1529 (vs), 1459 (s), 1193 (m, C–O), 1039 (m, C–N), 948 (s, VO), 836 (s), 757 (m, C–S). ^{1}H NMR (500 MHz, DMSO-d_6): 9.12 (s, 1H, CH═N), 8.50 (m, 6H), 8.00 (m, 3H), 7.78 (br m, 2H, ArH), 7.5 (br m, 2H, ArH), 6.96 (br m, 3H, ArH). UV–vis λ_{max}, nm (ε, $M^{-1}\,cm^{-1}$) in DMSO: 264 (41,770), 340 (15,255), 385 (6525). Magnetic moment: μ_{eff}: 1.68BM.

2.3.4. Synthesis of [VO (hntdtsc) (bpy)] (**2**)

This complex was synthesized by a similar procedure as for the complex **1**, with bpy (0.0781 g, 0.5 mmol) in place of 1,10-phennanthroline. Yield: 83.8%. Anal. Calcd. For $C_{22}H_{17}N_5O_2SV$: C, 56.65; H, 3.67; N, 15.02; S, 6.87%; Found: C, 56.36; H, 3.86; N, 14.88; S, 6.83%. ES-MS (CH_3OH, m/z): 467.0 (100%) ($[M+1]^+$). IR (KBr) (ν_{max}/cm^{-1}): 3428 (m), 3266 (m, $-NH_2$), 3064 (m, C–H), 1610 (vs), 1496 (vs), 1436 (w), 1187 (m, C–O), 1037 (m, C–N), 960 (s, VO), 879 (m), 738 (m, C–S). ^{1}H NMR (500 MHz, DMSO-d_6): 9.13 (s, 1H, CH═N), 8.69 (m, 4H), 8.39 (m, 5H), 7.95 (br m, 4H), 7.42 (br m, 3H, ArH). UV–vis λ_{max}, nm (ε, $M^{-1}\,cm^{-1}$) in DMSO: 264 (41,650), 341 (16,250), 376 (5322). Magnetic moment: μ_{eff}: 1.66BM.

2.3.5. Synthesis of [VO (satsc) (phen)] (**3**)

This complex was synthesized by a similar procedure as for the complex **1**, with satsc (0.0975 g, 0.5 mmol) in absolute methanol (30 mL) in place of hntdtsc in absolute methanol (100 mL). Yield: 57%. Anal. Calcd. For $C_{20}H_{15}N_5O_2SV$: C, 54.55; H, 3.43; N, 15.90; S, 7.28%; Found: C, 54.45; H, 3.69; N, 15.71; S, 7.21%. ES-MS (CH_3OH, m/z): 441.0 (100%) ($[M+1]^+$). IR (KBr) (ν_{max}/cm^{-1}): 3448 (s), 3288 (s, $-NH_2$), 3056 (w, C–H), 1603 (vs), 1541 (m), 1500 (s), 1433 (m), 1201 (m, C–O), 1043 (m, C–N), 945 (s, VO), 838 (s), 759 (w, C–S). ^{1}H NMR (500 MHz, DMSO-d_6): 9.11 (s, 1H, CH═N), 8.50 (m, 2H, ArH), 8.00 (br m, 3H), 7.84(br m, 5H), 6.81 (br m, 2H, ArH), 6.73 (br m, 2H, ArH). UV–vis λ_{max}, nm (ε, $M^{-1}\,cm^{-1}$) in DMSO: 265 (41,770), 346 (15,255), 375 (6525). Magnetic moment: μ_{eff}: 1.68BM.

2.3.6. Synthesis of [VO (satsc) (bpy)] (**4**)

This complex was synthesized by a similar procedure as for the complex **3**, with bpy (0.0781 g, 0.5 mmol) in place of 1, 10-phennanthroline. Yield: 49%. Anal. Calcd. For $C_{18}H_{15}N_5O_2SV$: C, 51.93; H, 3.63; N, 16.82; S, 7.70%; Found: C, 51.70; H, 3.89; N, 16.47; S, 7.67%. ES-MS (CH_3OH, m/z): 416.0 (95%) ($[M+1]^+$). IR (KBr) (ν_{max}/cm^{-1}): 3436 (s), 3276 (s, $-NH_2$), 3060 (w, C–H), 1611 (s), 1538 (m), 1497 (s), 1203 (m, C–O), 1047 (w, C–N), 941 (s, VO), 823 (s), 760 (s, C–S). ^{1}H NMR (500 MHz, DMSO-d_6): 8.69 (m, 3H), 8.40 (m, 4H), 7.94 (br m, 3H), 7.45 (br m, 3H, ArH), 7.22 (br, 1H, ArH), 6.85 (br, 1H, ArH). UV–vis λ_{max}, nm (ε, $M^{-1}\,cm^{-1}$) in DMSO: 265 (41,770), 345 (16,255), 381 (6435). Magnetic moment: μ_{eff}: 1.67BM.

2.4. DNA binding and cleavage

Absorption titrations of the oxidovanadium complexes in buffer A were performed using a fixed concentration of the oxidovanadium complex (20 μM) to which the DNA stock solutions were added. The oxidovanadium-DNA solutions were incubated at room temperature for 5 min before the absorption spectra were recorded. In order to further elucidate the binding strength of the complexes, the intrinsic binding constant K_b with CT-DNA was obtained by monitoring the change in the absorbance of the ligand transfer band with increasing amounts of DNA. K_b was then calculated using the following equation [29–35]:

$$\frac{[DNA]}{\varepsilon a-\varepsilon f}=\frac{[DNA]}{\varepsilon a-\varepsilon f}+\frac{1}{Kb(\varepsilon b-\varepsilon f)}$$

where [DNA] is the concentration of DNA in the base pairs, and ε_a, ε_f and ε_b refer to the corresponding apparent absorption coefficient A_{obsd}/[Vanadium], the extinction coefficient for the free oxidovanadium complex and the extinction coefficient for the oxidovanadium complex in the fully bound form, respectively. In plots of [DNA]/($\varepsilon_a-\varepsilon_f$) versus [DNA], K_b is obtained by the ratio of the slope to the intercept.

Viscosity measurements were carried out with an Ubbelohde viscometer maintained at a constant temperature of (28.0 ± 0.1) °C in a thermostatic bath. Flow time was measured with a digital stopwatch and each sample was measured five times to obtain the average flow time. Data are presented as $(\eta/\eta_0)^{1/3}$ versus binding ratio [28], where η is the viscosity of DNA in the presence of complexes while η_0 is the viscosity of DNA alone [30,33].

Thermal denaturation studies were carried out with Shimadzu UV-3101 PC spectrophotometer equipped with a Peltier temperature-controlling programmer (±0.1 °C). The melting curves were obtained by measuring the absorbance at 260 nm for solutions of CT-DNA (80 μM) in the absence and presence of oxidovanadium complex [20 μM] as a function of the temperature. The temperature was scanned from 50 to 90 °C at a speed of 5 °C min^{-1}.

The cleavage of supercoiled pBR322 DNA by the complexes was studied by the gel electrophoresis experiment, pBR322 DNA (0.1 μg) was treated with the oxidovanadium complexes in buffer B, and the

solution was incubated at 37 °C in the incubator. The samples were analyzed by electrophoresis for 1.5 h at 85 V on a 0.8% agarose gel in TBE (89 mM Tris-borate acid, 2 mM EDTA, pH = 8.3). The gel was stained with 1 μg/ml ethidium bromide and photographed on an Alpha Innotech IS-5500 fluorescence chemiluminescence and visible imaging system [33,34].

2.5. Antitumor assay in vitro

2.5.1. Cytotoxicity assays

The capacities of compounds to interfere with the growth of Myeloma cells (Ag8.653) and Gliomas cells (U251) were determined with the aid of MTT dye assay. Compounds were dissolved in DMSO and diluted with RPMI 1640 to the required concentrations prior to use. The control was well prepared by addition of culture medium (100 μL). Wells containing culture medium without cells were used as blanks. Myeloma cells (Ag8.653) and Gliomas cells (U251) with a density 2×10^4 cells per well were precultured into 96-well microtiter plates for 48 h at 37 °C, 5% CO_2. Upon completion of the incubation, then stock MTT dye solution was added to each well. After 4 h incubation, a solution containing N, N-dimethylformanmide (50%) sodium dodecyl sulfate (20%) was added to solubilize the MTT formazan. The cell viability was determined by measuring the absorbance of each well at 490 nm using a Multiskan SSCENT microplate reader. IC_{50} values were determined by plotting the percentage viability versus concentration on a logarithmic graph and reading off the concentration at which 50% of cells remain viable relative to the control [49–51].

2.5.2. Cell cycle analysis

Analysis of the cell cycle of control and treated cancer cells was determined. Using standard methods, the DNA of cells were stained with PI, and the proportion of non-apoptotic cells in different phases of the cell cycle was recorded [50,51]. The cancer cells were treated with the complex, harvested by centrifugation at $1000\times g$ for 5 min, and then washed with ice-cold PBS. The collected cells were fixed overnight with cold 70% ethanol, and then stained with PI solution consisting of 50 μg/mL PI, 10 μg/mL RNase. After 10 minute incubation at room temperature in the dark, fluorescence-activated cells were sorted in a FACScan flow cytometer using Cell Quest 3.0.1 software. The percentage of cells in each phase of the cell cycle was determined as least in triplicate and expressed as mean ± SD.

3. Results and discussion

3.1. Synthesis and characterization

The ligands, hntdtsc and satsc were prepared by the reaction of thiosemicarbazide with 2-hydroxy-1-naphthaldehyde and salicylaldehyde, respectively, in the appropriate mole ratios, using absolute methanol as the solvent [33–35]. The complexes [VO(hntdtsc)(phen)] (**1**), [VO(hntdtsc)(bpy)] (**2**), [VO(satsc)(phen)] (**3**) and [VO(satsc)(bpy)] (**4**) were prepared by refluxing of ligand, $VO(acac)_2$ with 1,10-phennanthroline and 2,2′-bipyridine in absolute methanol, respectively. The desired complexes were purified by recrystallization. The structures of these compounds were confirmed by elemental analysis, ES-MS, UV–vis, IR, and ^{1}H NMR spectroscopy. Synthetic routes of ligands and their complexes are shown in Scheme 1.

In the IR spectra of Schiff bases of thiosemicarbazone showed absorption bands at 3450–3167 cm^{-1} for (–NH_2) and (–NH–), at 2989–3053 cm^{-1} for aromatic (C–H), at 1593–1627 cm^{-1} for azomethine group (–CH═N) and (C═C), at 750–760 cm^{-1} confirms the group (–C═S) and at 1237–1240 cm^{-1} possible for group (C–O), But in the IR spectra of complexes, the peak of the azomethine group (–CH═N) has reduced by 14–19 cm^{-1} as compared with their ligands, respectively, which is assigned to the azomethine (–CH═N) coordinated to vanadium [16,28]. All other frequencies founded in the IR spectra of complexes are in accordance to the literature data for the same type of complexes [28,36–38].

In the ^{1}H NMR spectra of Schiff bases of thiosemicarbazone showed peaks of (NHCS), hydroxyl (OH), amine (NH_2) and imine (CH═N) proton. However, in the ^{1}H NMR spectra of complexes, the peaks of (NHCS) and hydroxyl (OH) were not observed, which affirmed that the free ligand was coordinated to vanadium.

In the electronic spectra, the complexes show an intense band at ca. 265 nm assignable to $\pi-\pi^*$ transitions of aromatic rings of phenanthroline [15,20,28,34]. A medium band is observed near 400 nm, which is attributed to a ligand-to-metal charge-transfer transition (LMCT) as a charge transfer from a *p*-orbital on the lone-pair of ligand oxygen atoms to the empty *d*-orbital of the vanadium atom [33]. The remaining bands appearing in the UV-region (320–350 nm) are assignable to the intraligand transitions of the Schiff base [15,16,33]. Complexes of oxidovanadium (IV) with coordination numbers 5 and 6 are usually square pyramidal/trigonal bipyramidal and distorted octahedral, respectively [14–19]. From the above obtained spectral data, it indicates that the Schiff bases bonded through the phenolate oxygen, imine nitrogen and thiolate sulfur atoms leaving the thiomethyl as the pendant group. This implies that these complexes bear the central V (IV) atom in a square-pyramidal geometry [16,17,33,38].

In the ES-MS spectra, for Schiff bases ligands showed peak at *m/z* 246.0 ($[M+1]^+$) (**hntdtsc**) and 196.0 ($[M+1]^+$) (**satsc**), respectively. The molecular ion peaks of complexes at *m/z* 491.0 ($[M+1]^+$) (**1**), 467.0 ($[M+1]^+$) (**2**), 441.0 ($[M+1]^+$) (**3**) and 417.0 ($[M+1]^+$) (**4**), respectively. Elemental analysis, ES-MS, IR and ^{1}H NMR data of all the compounds are in good agreement with the expected structures.

The molar conductance values of the four complexes in DMF are given in Table 1, which indicates these four oxidovanadium complexes show nonelectrolytic nature. As can be seen from Table 1, the complexes are one-electron paramagnetic giving a magnetic moment value of ~1.60 BM at room temperature. These values of magnetic susceptibility also confirm that the vanadium complexes are in the V (IV) states, with d^1 configuration [33,39,40].

3.2. DNA-binding studies

3.2.1. Electronic absorption titration

Electronic absorption spectroscopy is one of the most common ways to investigate the interaction of complexes with DNA. The intercalation of complexes into the base pairs of DNA usually results in hypochromism and bathochromism (red shift), which is correlated with the stacking interaction between the planar aromatic chromophore of complexes and the base pairs of DNA. The extent of the hypochromism is commonly consistent with strength of intercalative binding interaction [34,41,42].

For metallo-intercalators, DNA-binding is associated with hypochromism and a red shift in the MLCT and ligand bands [16,17]. Fig. 1 shows the absorption spectra of complexes (**1**), (**2**), (**3**) and (**4**) in the presence of increasing concentration of DNA. As can be seen in Fig. 1, upon increasing the CT-DNA concentration, appreciable hypochromism and bathochromism for the complexes **1** at 263.5 nm, **2** at 273 nm, **3** at 264 nm and **4** at 280.5 nm exhibit hypochromism of 29.7%, 25.7%, 24.3% and 19.3%, and bathochromism of 3 nm, 2.5 nm, 2 nm and 2 nm, respectively. According to previous reported results

Table 1
Conductivity and magnetic data of oxidovanadium complexes.

Compounds	Ω_M (Ω^{-1} cm^2 mol^{-1})	B.M (μ_{eff})
1	9.43	1.65
2	13.9	1.66
3	8.36	1.64
4	13.1	1.67

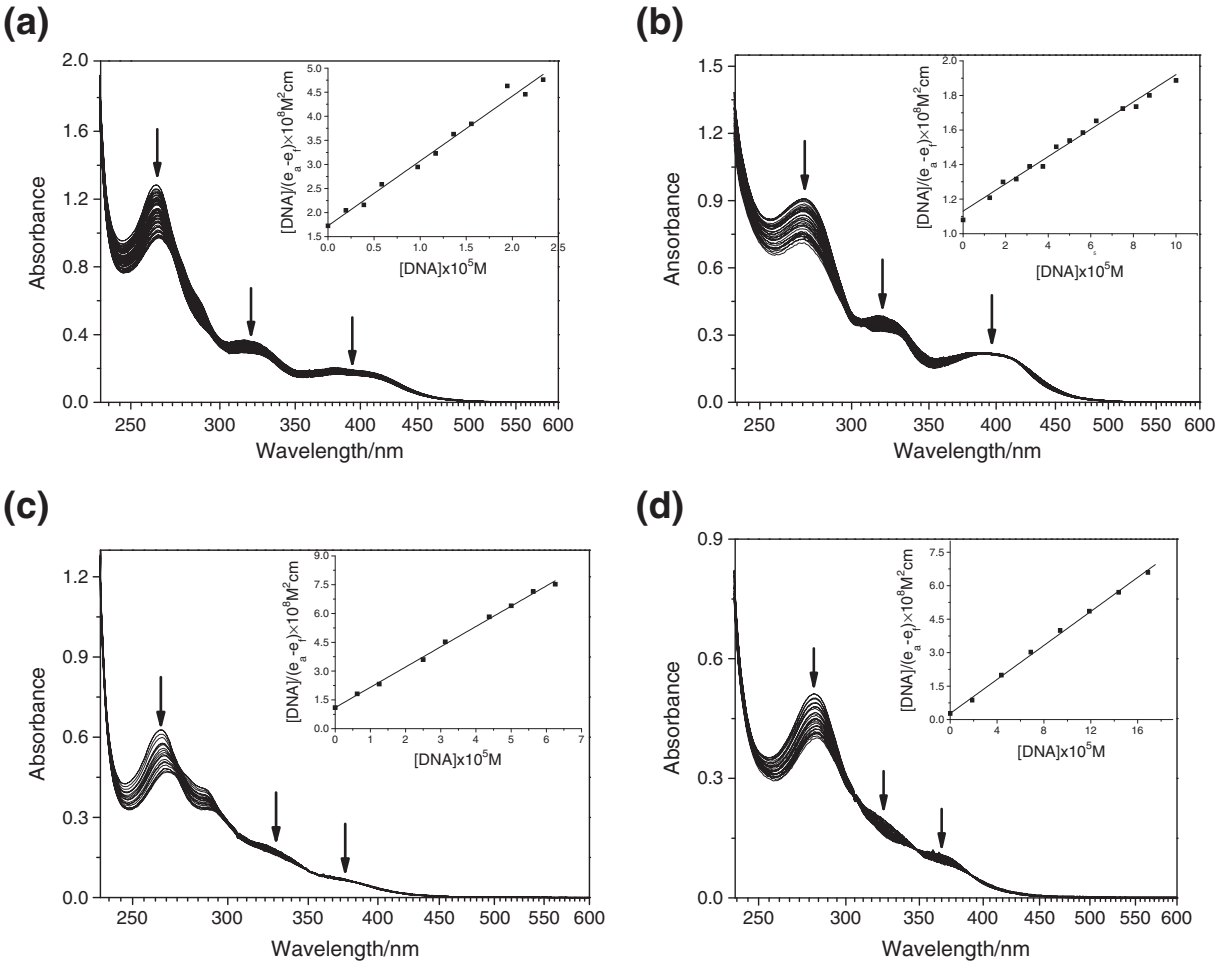

Fig. 1. Absorption spectral of the complexes **1** (a), **2** (b), **3** (c) and **4** (d) in Tris–HCl buffer A upon increasing amounts of CT-DNA. [V] = 20 μM, [DNA] = (0–100) μM. Arrow shows the decreasing absorbance upon increasing CT-DNA concentrations. Insert: Plots of [DNA]/(ε_a-ε_f) versus [DNA] for the titration of [V] with CT-DNA.

[9,34,43], these spectral characteristics obviously suggest that complexes **1**, **2**, **3** and **4** interact with DNA most likely through a mode that involves a stacking interaction between the aromatic chromophore and the base pairs of DNA.

In order to compare quantitatively the binding strength of these complexes with DNA, the intrinsic binding constant K_b was calculated by monitoring the changes of absorbance in the ligand transfer bands, with the increasing amounts of CT-DNA. The intrinsic binding constant K_b obtained for complexes **1**, **2**, **3** and **4** were $8.2\times10^4\ M^{-1}$, $7.8\times10^4\ M^{-1}$, $1.37\times10^4\ M^{-1}$ and $9.62\times10^3\ M^{-1}$, respectively. The K_b decreases in the order: **1** > **2** > **3** > **4**. The differences of their binding strength may be due to the presence of an appending aromatic moiety in **hntdtsc** and thus the larger binding affinities of the corresponding complexes in comparison with those complexes incorporating **satsc** [9,33,38,44]. The results also imply that the interactions of these complexes with DNA may be mainly through π — π stacking of **hntdtsc** and **satsc** plane and base-pairs, and show a classic intercalative mode. Meanwhile, the electronic effect of phenanthroline is one of the factors in determining the binding affinities.

3.2.2. Fluorescence spectroscopic studies

The interaction of the complexes with CT-DNA was studied using fluorescence emission titration experiment in the Tris buffer A at room temperature. The emission spectra of these four complexes in the absence and presence of CT DNA are shown in Fig. 2. As shown in Fig. 2, an obvious increase in emission intensity was observed for the four complexes. As increasing the concentration of CT-DNA, when the ratio of [DNA]/[V] of 11.67:1 for **1**, 9.73:1 for **2**, 6.81:1 for **3** and 5.84:1for **4** reached a saturating value, the emission intensities of complexes **1** (at 458 nm), **2** (at 458 nm), **3** (at 705 nm) and **4** (at 706 nm) grow to about 53%, 48%, 38% and 29 % larger than those in the absence of DNA, respectively. The enhancement of emission intensity is indicative of binding of the complexes to the hydrophobic pocket of DNA, since the hydrophobic environment inside the DNA helix reduces the accessibility of water molecules to the complex and the complex mobility is restricted at the binding site, leading to decrease of the vibrational modes of relaxation. These results are in agreement with the change in UV–vis spectra data.

3.2.3. Viscosity measurements

To further clarify the nature of the binding interaction between both complexes and DNA, viscosity measurements were carried out on CT DNA by varying the concentration of the added complexes. Spectroscopic data are necessary, but not sufficient to support a binding mode. Hydrodynamic measurements which are sensitive to length increase (for example, viscosity, sedimentation) are regarded as the least ambiguous and the most critical tests of binding in solution in the absence of crystallographic structure data [36–40]. A classical intercalative mode causes a significant increase in viscosity of DNA solution due to increase in separation of base pairs at intercalation sites and hence an increase in overall DNA length. In contrast, a partial, non-classical intercalation of compounds could bend (or kink) the DNA helix and reduce its effective length and, concomitantly, its viscosity [36,41–43].

The effects of complexes **1**, **2**, **3**, **4** and EB on the viscosity of CT-DNA are shown in Fig. 3. As can be seen in Fig. 3, upon increasing

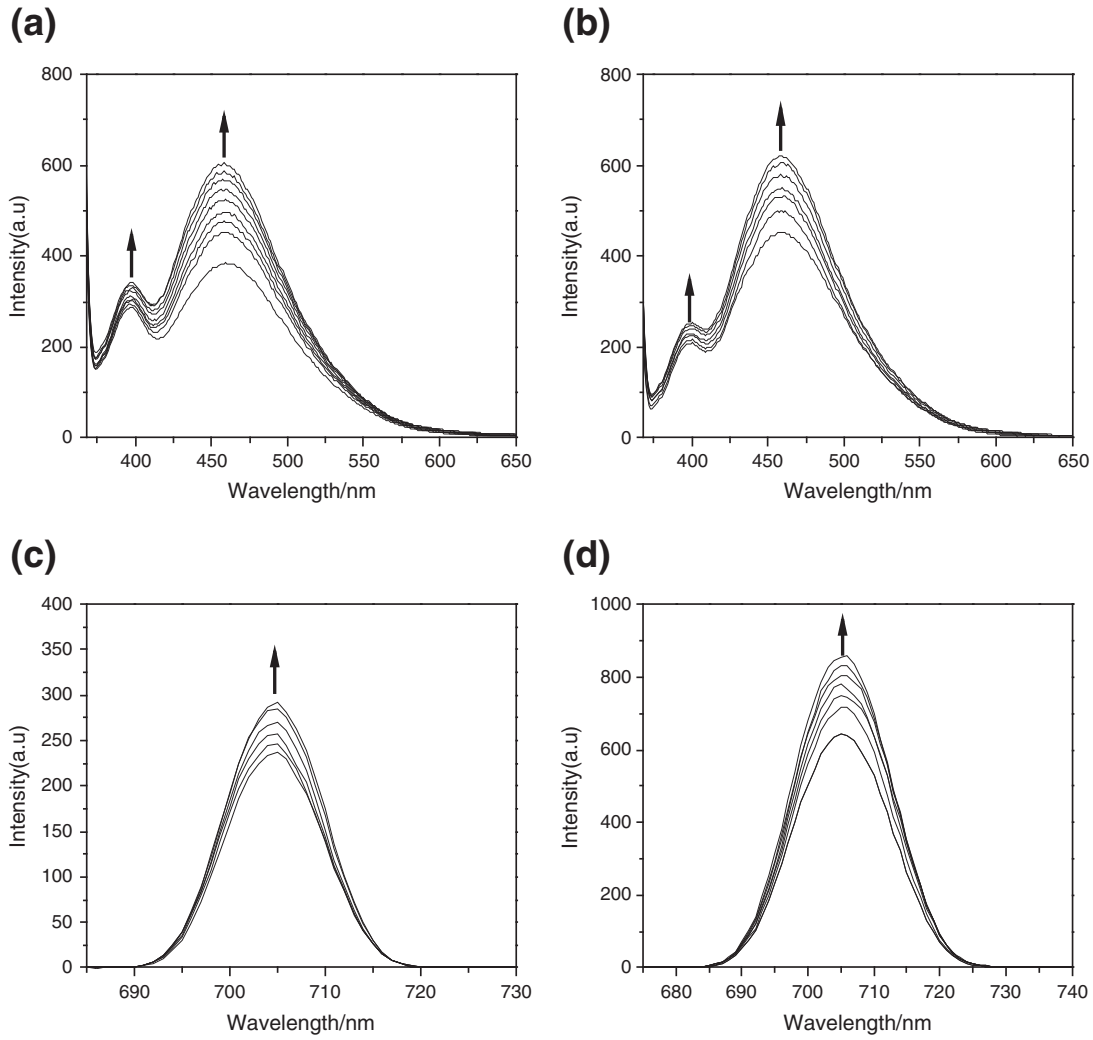

Fig. 2. Emission spectra of complexes **1** (a), **2** (b), **3** (c) and **4** (d) in Tris–HCl buffer A in the absence and presence of CT-DNA. [V] = 20 μM. Arrow shows the increasing intensity upon increasing DNA concentrations.

the amounts of complexes **1**, **2** and **3**, the relative viscosity of DNA increases steadily. The increasing degree of viscosity is **1** > **2** > **3** > **4**. The viscosity experimental results thus provide strong evidence for the interaction of complexes **1**, **2**, **3** and **4** with DNA by intercalation modes and the electronic effect of phenanthroline is an important factor in determining the intrinsic binding constant K_b.

3.2.4. Thermal denaturation studies

Thermal behaviors of DNA in the presence of compounds can give insight into their conformational changes when temperature is raised, and offer information about the interaction strength of complexes with DNA. Normally, when the temperature in the solution increases, the double-stranded DNA will gradually dissociate to single strands and generate a hyperchromic effect on the absorption spectra of DNA bases (λ_{Max} = 260 nm). The melting temperature T_m, which is defined as the temperature where half of the total base pairs are unbounded, is usually introduced. Generally, T_m will increase considerably when intercalative binding occurs, since intercalation of the complexes into DNA base pairs causes stabilization of base stacking and hence raises the melting temperature of the double-stranded DNA [36,39–43].

The changes of melting temperature of CT-DNA in the absence and presence of the complexes **1**, **2**, **3** and **4** are showed in Fig. 4. The T_m of CT-DNA in the absence of the complexes is 60.7 ± 0.2 °C. As can be seen from Fig. 4, when mixed with the compounds at a concentration ratio [V]/[DNA] of 1:4, the observed T_m in the presence of complexes **1**, **2**, **3** and **4** are 65.9 ± 0.2 °C, 64.5 ± 0.2 °C, 63.9 ± 0.2 °C and 63.7 ± 0.2 °C, respectively. The moderate increase in T_m (ΔT_m are 5.2 °C, 3.8 °C, 3.2 °C and 3.0 °C for **1**, **2**, **3** and **4**, respectively) was comparable

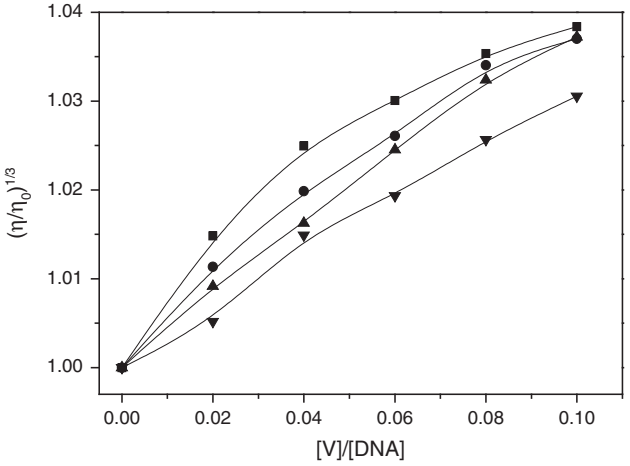

Fig. 3. Effects of increasing amounts of complexes **1** (■), **2** (●), **3** (▲) and **4** (▼) on the relative viscosity of CT-DNA at 28 (±0.1) °C. [DNA] = 0.40 mM.

to those observed for classical intercalate and lends strong support for their binding with DNA in intercalative modes [33,42–44]. The experiment results also show that complex **1** exhibits a larger DNA-binding affinity than that of complexes **2**, **3** and/or **4** does. It is consistent with their binding abilities with CT-DNA.

3.2.5. DNA cleavage

The cleavage reactions of complexes with plasmid DNA were monitored by agarose gel electrophoresis. The four complexes showed considerable DNA cleavage ability at low concentrations (15 μM) in the presence of H_2O_2. When circular plasmid DNA is subject to electrophoresis, relatively fast migration will be observed for the intact supercoiled form (Form I). If scission occurs on one strand (nicking), the supercoil form will relax to generate a slower moving open circular form (Form II). If both strands are cleaved, a linear form (Form III) that migrates between Forms I and II will be generated [29–32].

Figs. 5 and 6 show the cleavage of plasmid pBR322 DNA after incubation with different concentrations of oxidovanadium complexes at 37 °C for 1 h in the dark. Under the same conditions no cleavage of pBR 322 DNA occurred for H_2O_2 alone (lane 2 in Figs. 5 and 6, respectively). In the presence of the complexes **1**, **2**, **3**, and **4** with 30 mM H_2O_2 (lanes 3, 4 and 5 in Figs. 5 and 6, respectively) or 30 mM H_2O_2 and 0.02 M L-histamine being a singlet oxygen quencher (lanes 6 and 11 in Figs. 5 and 6, respectively), plasmid DNA was nicked, being evidently observed from the formation of From II, and for that L-Histamine slightly inhibits the cleavage of DNA. On the contrary, complete inhibition of DNA cleavage occurred in the presence of hydroxyl radical scavenger DMSO (lanes 7, 12 in Figs. 5 and 6, respectively), which suggests that •OH radical is likely to be the reactive species for the cleavage reaction. This can be explained by the generation of •OH radicals obtained from the oxidation of VO^{2+} in the presence of H_2O_2 through the reaction as follows: ($VO^{2+} + H_2O_2 \rightarrow VO_2^+ + {\bullet}OH + H^+$) [9,16–19]. These results indicate that the process of DNA cleavage may be closely related to the oxidation of vanadyl ions of oxidovanadium complexes and these four oxidovanadium complexes can degrade pBR322 DNA through oxidative cleavage in the presence of H_2O_2 [9,41,42]. Under comparative experimental conditions, the cleavage ability follows the order of **1**>**2**>**3**>**4**. This is consistent with the magnitude of their intrinsic binding constants (K_b), indicating that the photocleavage abilities might be closely related to the electronic effect of the ligands, which affected the binding ability as well.

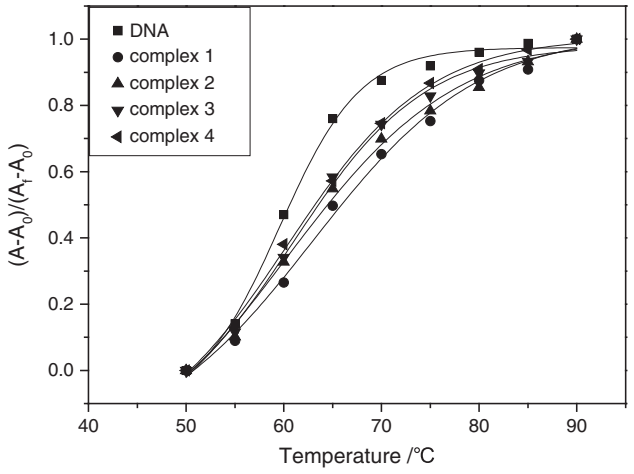

Fig. 4. Thermal denaturation of CT-DNA in the absence and presence of complexes **1**, **2**, **3** and **4**. [V] = 20 μM, [DNA] = 80 μM.

3.3. Antitumor assay in vitro

3.3.1. Cytotoxicity assays

The antitumor activity of all these complexes and the corresponding ligands against Ag8.653 and U251 cell lines was evaluated by MTT assay [45–48]. The IC_{50} values obtained of ligands and their complexes against selected two tumor cell lines are shown in Table 2. The histogram of cell viability assay for different compounds against selected tumor cells obtained with continuous exposure for 48 h is shown in Fig. 8. As shown in Table 2 and Fig. 8, the synthetic oxidovanadium complexes exhibit broad inhibition on the two tested human cancer cell lines with the IC_{50} values ranging from 0.004 to 0.950 μM, respectively. The results also indicate that all of these oxidovanadium complexes and their corresponding ligands exhibit antitumor activities against the selected cell lines in different concentrations and the antitumor activities are concentration-dependent [16,18]. With comparison of the antitumor activities of the ligands and corresponding complexes, oxidovanadium complexes appeared to be much cytotoxic against the cell lines of Ag8.653 and U251. Fig. 7 shows the antiproliferative activity in the absence (I) and presence of complexes **1** (II), **2** (III), **3** (IV) and **4** (V), at the concentration of 200 μM. As shown in Fig. 7, the proliferation of tumor cells of Ag8.653 was effectively inhibited.

It is notable that complex **1**, as compared with other tested complexes, possessed the most potent inhibitory effect against the two cell lines. And its IC_{50} value which is very close to that of cisplatin indicated its high cytotoxic effects against human cancer cells. This is consistent with its binding abilities with CT DNA, indicating that the antitumor abilities of the oxidovanadium complexes may be closely related to their DNA binding mode.

3.3.2. Cell cycle analysis

In order to further define the mechanism of anti-proliferative effect of oxidovanadium complexes on tumor cells, the cell cycle phase distribution was analyzed by flow cytometry with PI staining [16,49–51]. According to the results of Table 3, Ag8.653 cells exhibited the higher sensitivity to complex **1**. Thus this cell line was used for further investigation on the underlying mechanisms accounting for the antiproliferative action of complex **1**. The Ag8.653 cells were treated with 0.001 μM, 0.002 μM and 0.004 μM of complex **1** for 48 h, respectively. As shown in Table 3, the G2/M phase was arrested significantly after Ag8.653 cells were exposed to 0.004 μM (IC_{50} values) complex **1** for 48 h. Treatment with 0.001 or 0.002 μM complex **1** resulted in modest G2/M phase arrest of Ag8.653 cells at 48 h time point. The results in this work showed that there were significantly decreased G0/G1 phase distribution and increased G2/M phase distribution in a dose-dependent manner, indicating the induction of G0/G1-phase arrest by complex **1**. Moreover, apoptotic cells and cell debris significantly increased after Ag8.653 cells were exposed to the complex **1**. In conclusion, the results suggested that oxidovanadium complexes induced proliferative suppression of Ag8.653 cells were via the induction of apoptosis [47,49,51]. To fully understand the mechanism involved in the induction of apoptosis by

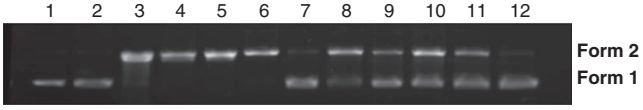

Fig. 5. Cleavage of pBR322 DNA by oxidovanadium complexes **1** and **3** (15–60 μM) in the absence and presence of H_2O_2 (30 mM) in buffer B (pH 7.2). Lane 1, DNA control; lane 2, DNA + H_2O_2; lane 3, DNA + **1** (15 μM) + H_2O_2; lane 4, DNA + **1** (30 μM) + H_2O_2; lane 5, DNA + **1** (60 μM) + H_2O_2; lane 6, DNA + **1** (30 μM) + H_2O_2 + L-Histidine (0.02 M); lane 7, DNA + **1** (30 μM) + H_2O_2 + DMSO (2 μL); lane 8, DNA + **3** (15 μM) + H_2O_2; lane 9, DNA + **3** (30 μM) + H_2O_2; lane 10, DNA + **3** (60 μM) + H_2O_2; lane 11, DNA + **3** (30 μM) + H_2O_2 + L-Histidine (0.02 M); lane 12, DNA + **3** (30 μM) + H_2O_2 + DMSO (2 μL).

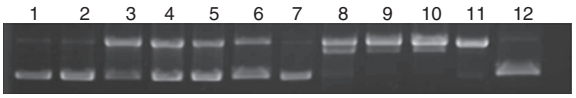

Fig. 6. Cleavage of pBR322 DNA by oxidovanadium complexes **2** and **4** (15–60 μM) in the absence and presence of H_2O_2 (30 mM) in buffer B (pH 7.2). Lane 1, DNA control; lane 2, DNA + H_2O_2; lane 3, DNA + **2** (15 μM) + H_2O_2; lane 4, DNA + **2** (30 μM) + H_2O_2; lane 5, DNA + **2** (60 μM) + H_2O_2; lane 6, DNA + **2** (30 μM) + H_2O_2 + L-Histidine (0.02 M); lane 7, DNA + **2** (30 μM) + H_2O_2 + DMSO (2 μL); lane 8, DNA + **4** (15 μM) + H_2O_2; lane 9, DNA + **4** (30 μM) + H_2O_2; lane 10, DNA + **4** (60 μM) + H_2O_2; lane 11, DNA + **4** (30 μM) + H_2O_2 + L-Histidine (0.02 M); lane 12, DNA + **4** (30 μM) + H_2O_2 + DMSO (2 μL).

oxidovanadium complexes, further investigation will be needed to be carried out.

4. Conclusion

Four oxidovanadium complexes, [VO(hntdtsc)(phen)] (**1**), [VO(hntdtsc)(bpy)] (**2**), [VO(satsc)(phen)] (**3**) and [VO(satsc)(bpy)] (**4**) have been synthesized and characterized by elemental analysis, ES-MS, IR, ^{1}H NMR, UV–vis and magnetic moment measurement. Their DNA-binding activities were investigated using spectroscopic methods, viscosity measurements and thermal denaturation. The experimental results show that these four oxidovanadium complexes bind to CT-DNA by intercalation modes and the DNA-binding affinity follows the order **1** > **2** > **3** > **4**. These oxidovanadium complexes show efficiently oxidative cleavage of supercoiled plasmid DNA in the presence of H_2O_2. In addition, these complexes present cytotoxic activities against Ag8.653 and U251 cell lines. Complex **1** exhibits a promising compound with a potential in treatment of cancers. Further work is in progress to better identify the active species in solution and to prepare more potent and stable related oxidovanadium compounds.

Table 2
The IC_{50} values for hntdtsc, satsc, **1**, **2**, **3** and **4** against Ag8.653 and U251 cell lines.

Compounds	IC_{50} (μM)	
	Ag8.653	U251
Cisplatin	0.002 ± 0.001	0.005 ± 0.001
hntdtsc	2.034 ± 0.332	5.210 ± 0.217
satsc	22.384 ± 4.733	25.543 ± 2.195
1	0.004 ± 0.001	0.007 ± 0.001
2	0.296 ± 0.081	0.134 ± 0.079
3	0.369 ± 0.097	0.203 ± 0.068
4	0.950 ± 0.081	0.524 ± 0.029

Cells were treated with various concentrations of tested compounds for 48 h. Cell viability was determined by MTT assay and IC50 values were calculated as described in Materials and Methods. Each value represents the mean ± SD of three independent experiments.

Abbreviations

MTT	3-(4,5-dimethylthiazoyl-2-yl) 2, 5-diphenyltetrazoliumbromide;
IC_{50}	50% inhibition concentrations;
Tm	the DNA-melting temperature where total base pairs are unbound;
ES-MS	electrospray mass spectra;
Hntdtsc	2-hydroxy-1-naphthaldehyde thiosemicarbazone;
Satsc	salicylaldehyde thiosemicarbazone;

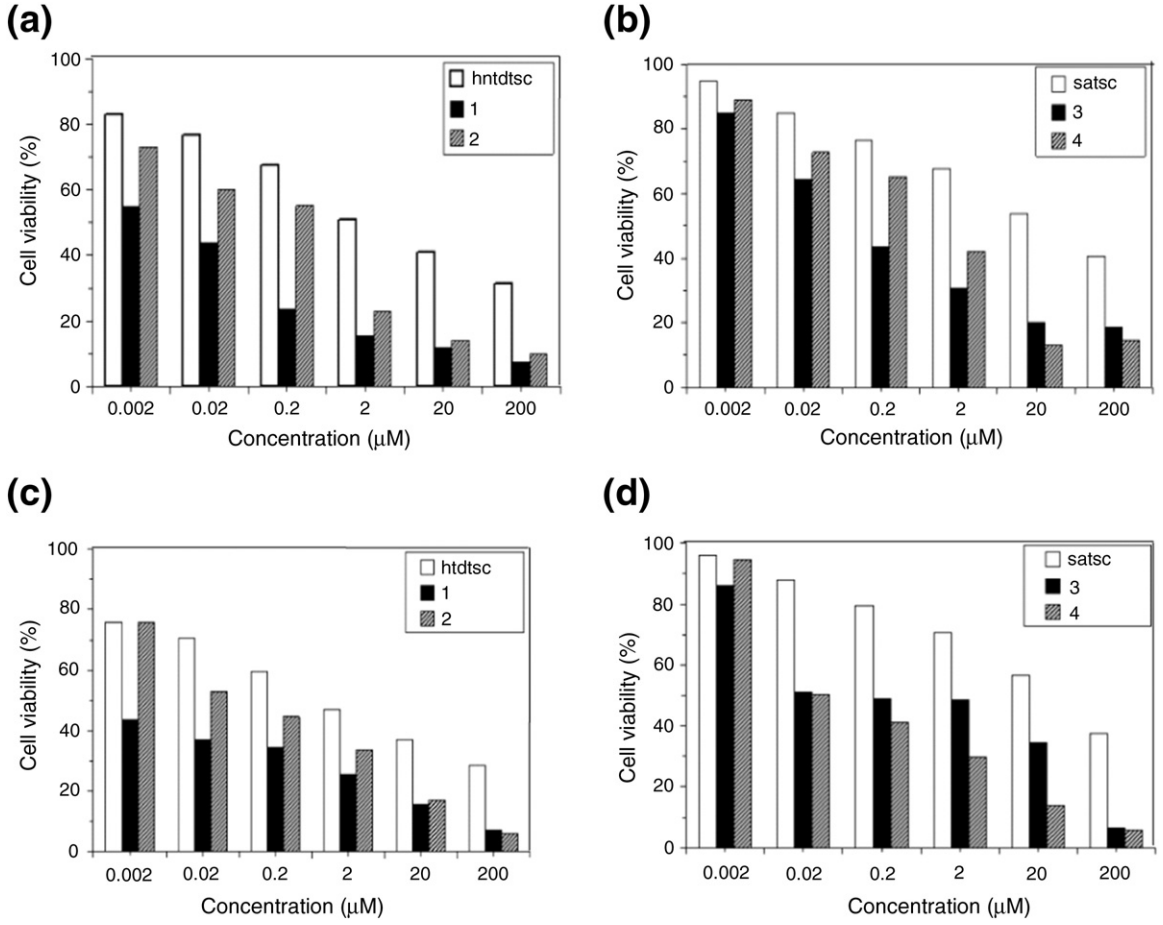

Fig. 7. Cell viability of **hntdtsc**, **satsc**, **1**, **2**, **3** and **4** on tumor Ag8.653 (a, b) and U251 (c, d) cells proliferation in vitro. Each data point is the mean ± standard error obtained from three independent experiments.

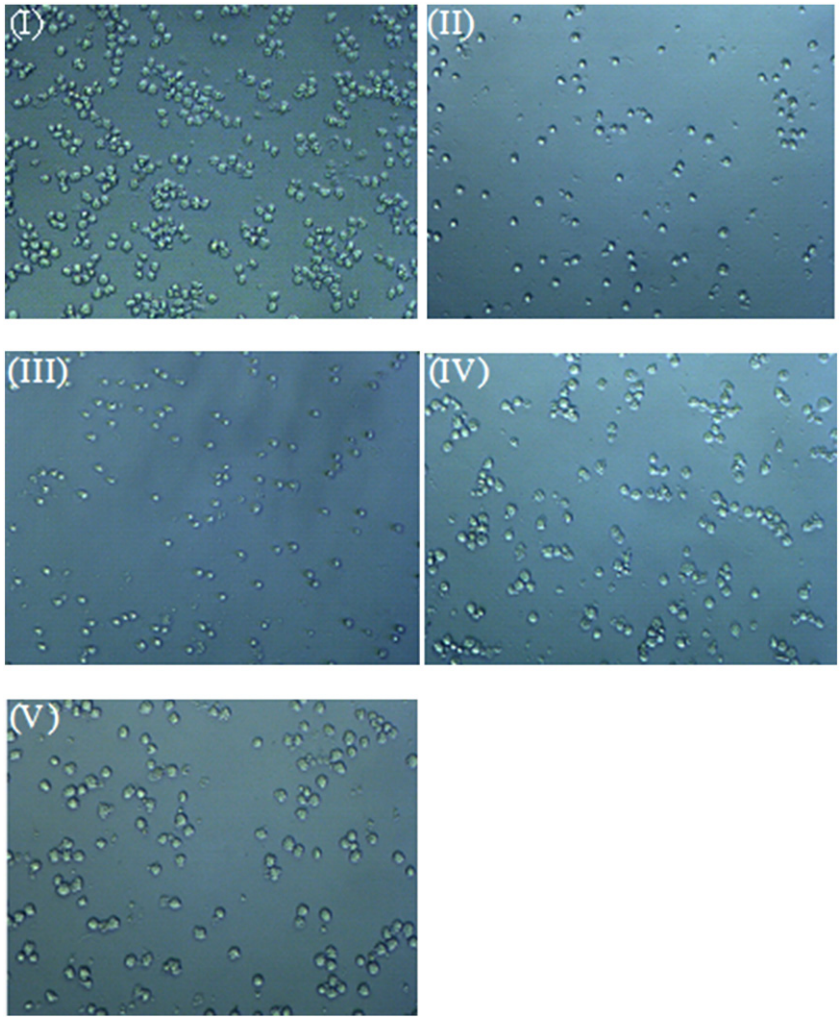

Fig. 8. Micrograph of the myeloma tumor (Ag8.653) cell line after treated for 48 h in the absence (I) (control) and presence of complexes **1** (II), **2** (III), **3** (IV) and **4** (V), respectively, [V] = 200 μM. Cell was observed using an inverted microscope and photographed by a digital camera.

Phen 1,10-phenanthroline;
Bpy 2,2′-bipyridine;
Acac acetylacetonate;
CT-DNA calf thymus DNA;
DMF N,N-Dimethyformamide;

Acknowledgments

We gratefully acknowledge financial support for this work by Guangdong Pharmaceutical University (No. 43540119), the National Key Research Project of China (No. 2011zx09102-001-31) and the National Natural Science Foundation of P. R. China (Nos. 81102753 and 21101033).

Table 3
The cell cycle analysis of the Ag8.653 cells induced by complex **1**.

Concentration	The relative proportion of different phase in the cell cycle (%)			
(μM)	G0/G1	G2/M	S	APO
Control	69.22 ± 3.52	9.40 ± 0.65	20.36 ± 3.40	0.43 ± 0.16
0.001	57.00 ± 3.92*	15.08 ± 0.95**	20.92 ± 1.77	4.03 ± 2.16*
0.002	55.10 ± 3.74**	20.87 ± 2.89**	20.50 ± 2.16	5.33 ± 1.82**
0.004	42.95 ± 1.78**	25.32 ± 3.89**	19.61 ± 2.84	7.22 ± 1.92**

Data are the mean ± SD of at least three independent experiments.
* $P<0.05$ versus the control, the difference was significant.
** $P<0.01$ versus the control, the difference was markedly significant.

References

[1] W.X. Hu, W. Zhou, C.N. Xia, X. Wen, Bioorg. Med. Chem. Lett. (2006) 2213.
[2] I. Dilovic, M. Rubcic, V. Vrdoljak, S.K. Pavelic, I. Piantanida, M. Cindric, Bioorg. Med. Chem. 16 (2008) 5189–5198.
[3] A.A. El-Asmy, O.A. Al-Gammal, D.A. Saad, S.E. Ghazy, J. Mol. Struct. 934 (2009) 9–22.
[4] Y.J. Liu, C.H. Zeng, Transit. Met. Chem. 34 (2009) 455–462.
[5] K.H. Thompson, J.H. McNeill, C. Orvig, Chem. Rev. 99 (1999) 2561–2571.
[6] D.L. Arockiasamy, S. Radhika, R. Parthasarathi, B.U. Nair, Eur. J. Med. Chem. 44 (2009) 2044–2051.
[7] R. Blasius, C. Moucheron, A.K. Mesmasker, Eur. J. Inorg. Chem. (2004) 3971–3979.
[8] Y. Xiong, L.N. Ji, Coord. Chem. Rev. 185 (1999) 711–733.
[9] L. Leelavathy, S. Anbu, M. Kandaswamy, N. Karthikeyan, N. Mohan, Polyhedron 28 (2009) 903–910.
[10] N. Shahabadi, S. Kashanian, M. Purfoulad, Spectrochim. Acta A Mol. Biomol. Spectrosc. 72 (2009) 757–761.
[11] A. Bishayee, A. Waghray, M.A. Patel, Cancer Lett. 294 (2010) 1–12.
[12] E.K. Efthimiadou, N. Katsaros, A. Karaliota, Bioorg. Med. Chem. Lett. 17 (2007) 1238–1242.
[13] B.T. Thaker, K.R. Surati, C.K. Modi, Russ. J. Coord. Chem. 34 (2008) 25–33.
[14] M.-J. Xie, Y.-F. Niu, X.-D. Yang, W.-P. Liu, L. Li, L.-H. Gao, S.-P. Yan, Z.-H. Meng, Eur. J. Med. Chem. 45 (2010) 6077–6084.
[15] I.C. Mendes, L.M. Botion, A.V.M. Ferreira, Inorg. Chim. Acta 362 (2009) 414–420.
[16] J. Benítez, L. Guggeri, I. Tomaz, J. Costa Pesso, V. Moreno, J. Lorenzo, F.X. Avilés, B. Garat, D. Gambino, J. Inorg. Biochem. 103 (2009) 1386–1394.
[17] J. Benítez, L. Guggeri, I. Tomaz, G. Arrambide, M. Navarro, J. Costa Pessoa, B. Garat, D. Gambino, J. Inorg. Biochem. 103 (2009) 609–616.

[18] J. Benítez, L. Becco, I. Correia, S.M. Leal, H. Guiset, J.C. Pessoa, S. Tanco, P. Escobar, V. Moreno, B. Garat, D. Gambino, J. Inorg. Biochem. 105 (2011) 303–312.
[19] Maia P.I.d.S., F.R. Pavan, C.Q.F. Leite, Polyhedron 28 (2009) 398–406.
[20] J.H. Wang, R.K. Larson, M. Mahdi, Inorg. Chem. 42 (2003) 7967–7977.
[21] H.L. Wu, K. Li, T. Sun, Trans. Met. Chem. 36 (2011) 21–28.
[22] S. Satyanarayana, J.C. Daborusak, J.B. Chaires, Biochemistry 32 (1993) 2573–2584.
[23] T. Uno, K. Hamasaki, M. Tannigawa, S. Shimabayashi, Inorg. Chem. 36 (1997) 1676–1682.
[24] F.R. Pavan, P.I. da S. Maia, S.R.A. Leite, V.M. Deflon, A.A. Batista, D.N. Sato, S.G. Franzblau, C.Q.F. Leite, Eur. J. Med. Chem. 45 (2010) 1898–1905.
[25] Q.L. Zhang, J.G. Liu, H. Li, Inorg. Chim. Acta 339 (2002) 34–39.
[26] A.M. Evangelou, Crit. Rev. Oncol. Hematol. 42 (2002) 249–265.
[27] D. Rehder, Inorg. Chem. Commun. 6 (2003) 604–617.
[28] N. Raman, A. Selvan, J. Mol. Struct. 985 (2011) 173–183.
[29] P. Zhao, L.C. Xu, J.W. Huang, B. Fu, H.C. Yu, L.N. Ji, Biophys. Chem. 135 (2008) 102–109.
[30] P. Zhao, L.C. Xu, J.W. Huang, B. Fu, H.C. Yu, L.N. Ji, Spectrochim. Acta A Mol. Biomol. Spectrosc. 71 (2008) 1216–1223.
[31] P. Zhao, L.C. Xu, J.W. Huang, B. Fu, H.C. Yu, L.N. Ji, Bioorg. Chem. 36 (2008) 278–287.
[32] N. Kurita, K. Kobayashi, Comput. Chem. 24 (2000) 351–355.
[33] J.Z. Lu, Y.F. Du, H.W. Guo, J. Coord. Chem. 64 (7) (2011) 1229–1239.
[34] Y.F. Du, J.Z. Lu, H.W. Guo, J. Jiang, Trans. Met. Chem. 35 (2010) 859–864.
[35] C.Z. Li, J.G. Wu, L.F. Wang, R. Min, J. Inorg. Biochem. 73 (1999) 195–202.
[36] P. Prasad, P.K. Sasmal, R. Majumdar, R.R. Dighe, A.R. Chakravarty, Inorg. Chim. Acta 363 (2010) 2743–2751.
[37] P.K. Sasmal, A.K. Patra, M. Nethaji, A.R. Chakravarty, Inorg. Chem. 46 (2007) 11112–11121.
[38] L.Z. Li, Z.H. Guo, Q.F. Zhang, T. Xu, D.Q. Wang, Inorg. Chem. Commun. 13 (2010) 1166–1169.
[39] V. Vrdoljak, I. Dilović, M. Rubčić, S.K. Pavelić, M. Kralj, D. Matković-Calogović, I. Piantanid, P. Novak, A. Rozman, M. Cindrić, Eur. J Med. Chem. 45 (2010) 38–48.
[40] J.C. Pessoa, I. Cavaco, I. Correia, I. Tomaz, M.T. Duarte, P.M. Matias, J. Inorg. Biochem. 80 (2000) 35–39.
[41] G. Micera, V.L. Pecoraro, E. Garribba, Inorg. Chem. 48 (2009) 5790–5796.
[42] N. Butenko, A.I. Tomaz, O. Nouri, E. Escribano, V. Moreno, S. Gama, V. Ribeiro, J.P. Telo, J. Costa Pessoa, I. Cavaco, J. Inorg. Biochem. 103 (2009) 622–632.
[43] B.E. Smith, T.D. Lash, Tetrahedron 66 (2010) 4413–4422.
[44] A. McCrate, M. Carlone, M. Nielsen, S. Swavey, Inorg. Chem. Commun. 13 (2010) 537–539.
[45] Y.J. Liu, C.H. Zeng, Eur. J. Med. Chem. 45 (2010) 3087–3095.
[46] G. Klopman, J. Am. Chem. Soc. 90 (1968) 223–229.
[47] A. Klein, P. Holko, J. Ligeza, A.M. Kordowiak, Folia Biol. 56 (2008) 115–121.
[48] I. Vermes, C. Haanen, H. Steffens-Nakken, C. Reutelingsperger, J. Immunol. Methods 184 (1995) 39–51.
[49] R. Kim, Cancer 103 (2005) 1551–1558.
[50] R.S. Ray, B. Rana, B. Swami, V. Venu, M. Chatterjee, Chem. Biol. Interact. 163 (2006) 239–247.
[51] I. Kostova, Anticancer Agents Med. Chem. 9 (2009) 827–842.